Experimental Neurology 351 (2022) 113994

Contents lists available at ScienceDirect

Experimental Neurology

journal homepage: www.elsevier.com/locate/yexnr

Research paper

Mice lacking full length Adgrb1 (Bai1) exhibit social deficits, increased seizure susceptibility, and altered brain development

Fu Hung Shiu [a,b], Jennifer C. Wong [a], Takahiro Yamamoto [c], Trisha Lala [b,d], Ryan H. Purcell [e], Sharon Owino [d], Dan Zhu [f], Erwin G. Van Meir [c,g], Randy A. Hall [d], Andrew Escayg [a,*]

[a] Department of Human Genetics, Emory University School of Medicine, Atlanta, GA, USA
[b] Neuroscience Graduate Program, Graduate Division of Biological and Biomedical Sciences, Laney Graduate School, Emory University, Atlanta, GA, USA
[c] Department of Neurosurgery, School of Medicine, University of Alabama at Birmingham (UAB), Birmingham, AL, USA
[d] Department of Pharmacology and Chemical Biology, Emory University School of Medicine, Atlanta, GA, USA
[e] Department of Cell Biology, Emory University School of Medicine, Atlanta, GA, USA
[f] Department of Neurosurgery, Emory University School of Medicine, Atlanta, GA, USA
[g] O'Neal Comprehensive Cancer Center, University of Alabama at Birmingham (UAB), Birmingham, AL, USA

ARTICLE INFO

Keywords:
BAI1
Seizures
Epilepsy
Autism
GPCR

ABSTRACT

The adhesion G protein-coupled receptor BAI1/ADGRB1 plays an important role in suppressing angiogenesis, mediating phagocytosis, and acting as a brain tumor suppressor. BAI1 is also a critical regulator of dendritic spine and excitatory synapse development and interacts with several autism-relevant proteins. However, little is known about the relationship between altered BAI1 function and clinically relevant phenotypes. Therefore, we studied the effect of reduced expression of full length Bai1 on behavior, seizure susceptibility, and brain morphology in *Adgrb1* mutant mice. We compared homozygous (*Adgrb1*$^{-/-}$), heterozygous (*Adgrb1*$^{+/-}$), and wild-type (WT) littermates using a battery of tests to assess social behavior, anxiety, repetitive behavior, locomotor function, and seizure susceptibility. We found that *Adgrb1*$^{-/-}$ mice showed significant social behavior deficits and increased vulnerability to seizures. *Adgrb1*$^{-/-}$ mice also showed delayed growth and reduced brain weight. Furthermore, reduced neuron density and increased apoptosis during brain development were observed in the hippocampus of *Adgrb1*$^{-/-}$ mice, while levels of astrogliosis and microgliosis were comparable to WT littermates. These results show that reduced levels of full length Bai1 is associated with a broader range of clinically relevant phenotypes than previously reported.

1. Introduction

Brain-specific angiogenesis inhibitor (BAI1/ADGRB1) is a member of the adhesion G protein-coupled receptor (GPCR) family (Duman et al., 2016; Purcell and Hall, 2018). Besides sharing a well-conserved seven-transmembrane structure with other GPCRs, BAI1 also features a large N-terminal extracellular domain with five thrombospondin type 1 repeats (TSRs) and a GPCR-autoproteolysis-inducing (GAIN) domain (Cork and Van Meir, 2011; Stephenson et al., 2014). BAI1 suppresses angiogenesis (Cork et al., 2012; Kaur et al., 2009; Zhu et al., 2012), mediates engulfment of apoptotic cells and gram-negative bacteria (Das et al., 2011; Park et al., 2007; Sokolowski et al., 2011), promotes myogenesis (Hochreiter-Hufford et al., 2013), and serves as a brain tumor suppressor by stabilizing p53 (Zhu et al., 2018). Although BAI1 was first associated with non-neuronal functions, the receptor is most abundantly expressed in neurons and glia in the cortex, hippocampus, thalamus, amygdala, and striatum (Sokolowski et al., 2011; Zhang et al., 2014). *Adgrb1* mRNA expression peaks at postnatal day 10 (P10) in rodents and expression is maintained into adulthood (Kee et al., 2004).

Studies during the past decade indicate that *in vitro* and *in vivo* knockdown of Bai1 leads to the formation of more immature and unstable dendrites (Duman et al., 2019; Duman et al., 2013), while overexpression of Bai1 results in dendrite retraction (Duman et al., 2019). Mice lacking full-length Bai1 display reduced expression of post-synaptic density 95 (PSD-95) (Zhu et al., 2015), a protein that regulates synaptic stability and plasticity (Cheng et al., 2006). The continuous morphological modifications of dendrites and proper PSD-95 function are essential for learning and memory (Coley and Gao, 2018;

* Corresponding author.
E-mail address: aescayg@emory.edu (A. Escayg).

https://doi.org/10.1016/j.expneurol.2022.113994
Received 8 July 2021; Received in revised form 20 December 2021; Accepted 24 January 2022
Available online 31 January 2022

Migaud et al., 1998) and are often altered in neurodevelopmental and neurological disorders characterized by impaired social interaction, communication deficits, and increased repetitive behaviors (Lin and Koleske, 2010; Penzes et al., 2011; Tsai et al., 2012). Consistent with this observation, *Adgrb1*$^{-/-}$ mice exhibit deficits in spatial memory and alterations in synaptic plasticity that are reflected by enhanced long-term potentiation (LTP) and reduced long-term depression (LTD) (Zhu et al., 2015).

De novo rare variants in *ADGRB1* have been identified in patients with autism spectrum disorder (ASD) (Satterstrom et al., 2020). A substantial percentage of individuals with ASD (8–24%) have epilepsy and exhibit altered brain morphology and developmental delay (Amiet et al., 2008; Gabis et al., 2005; Ghacibeh and Fields, 2015). These behavioral phenotypes are also observed in animal models of ASD (Sierra-Arregui et al., 2020; Varghese et al., 2017). Furthermore, BAI1 interacts with autism-relevant proteins, including BAIAP2/IRSp53 and Neuroligin-1 (NLG1) (De Rubeis et al., 2014; Nakanishi et al., 2017; Oda et al., 1999), although little is known about the functional significance of these interactions. Therefore, in the current study, we investigated the *in vivo* physiological role of BAI1 by characterizing the behavioral and seizure phenotypes of homozygous mice lacking full-length Bai1 (*Adgrb1*$^{-/-}$) and heterozygous mice (*Adgrb1*$^{+/-}$) that express approximately 50% of wild-type levels. Our results indicate that *Adgrb1*$^{-/-}$ mice exhibit impairments in sociability, social discrimination, and increased seizure susceptibility. *Adgrb1*$^{-/-}$ mice also display increased apoptosis during brain development, reduced brain weight, and reduced hippocampal neuron density.

2. Material and methods

2.1. Animals

The generation and genotyping of mice lacking full-length Bai1 were previously described (Zhu et al., 2015). These mice were engineered with a deletion of exon 2 (where the ATG start codon is located) and fail to express full length Bai1. Heterozygous mutants (*Adgrb1*$^{+/-}$) on a C57BL/6J (000664, Jackson laboratory) background were bred to generate wild-type (WT), heterozygous (*Adgrb1*$^{+/-}$), and homozygous (*Adgrb1*$^{-/-}$) offspring. Mice were housed in groups of 3–5 on a 12-h light/dark cycle with standard laboratory rodent chow (5001, Lab Diet) and water available *ad libitum*. All experiments were performed in accordance with the Emory University Institutional Animal Care and Use Committee (IACUC) guidelines.

2.2. Survival and body growth curve analysis

Male and female *Adgrb1*$^{-/-}$, *Adgrb1*$^{+/-}$ and WT littermates were weighed once every two days from postnatal day 7 to 24 (P7 – P24) and then once a week until P65 (n = 9–15/group).

2.3. Brain weight assessment

Male and female mice of all genotypes at three different ages (P1, 3 weeks, 2–3 months) were weighed and anesthetized with isoflurane. Brains were harvested and immediately weighed (n = 8–19/group).

2.4. Immunofluorescence staining and imaging

Brains were postfixed in 4% PFA overnight at 4 °C and then transferred to 30% sucrose solution in phosphate-buffered saline (PBS). Coronal sections (40 μm) were stained with antibodies against GFAP (1:400, 13–0300, Thermo Fischer), IBA1 (1:400, Ab178846, Abcam), NeuN (1:1000, MAB377, Millipore), and cleaved-caspase-3 (CC3) (1:200, 9664, Cell Signaling Technology). Goat anti-Mouse IgG (1:500, ab150114, Abcam) and goat anti-Rat IgG (1:500, A-21434, Thermo Fischer) were used as the secondary antibodies for NeuN and GFAP, respectively. Goat anti-Rabbit IgG (1:500, ab150077, Abcam) was used as the secondary antibody for IBA1 and CC3. Slides were washed multiple times with PBS and incubated with appropriate fluorescently labeled secondary antibodies for 1 h at 37 °C. For NeuN, GFAP, and IBA1 staining, confocal images were acquired on an Olympus FV1000 inverted microscope using the Olympus Fluoview v4.2 software. For CC3 staining, an upright microscope (DM6000B, Leica) was used. Three sections per mouse containing the hippocampus and primary somatosensory cortex (bregma −1.96 mm) were used for immunofluorescence staining. NeuN positive cells in the dentate gyrus (DG) and CA1 were counted per mm^2. CC3 positive (CC3+) cells were counted in the DG, CA1, and primary somatosensory cortex. GFAP and IBA1 immunoreactivity (IR) were calculated as the percentage area of the total region of interest (ROI) of the DG and CA1 using ImageJ (NIH). A threshold for IR was determined across all antibody images as previously described (Chalermpalanupap et al., 2018). The IR area within the ROI and the total area of the ROI were calculated using the "Measure" feature of ImageJ, and the percent area of IR was determined (area of IR within ROI divided by the total area of ROI and multiplied by 100). Two sections per mouse containing the rostral hippocampus were used for P1 mice. Similarly, CC3+ cells were counted in the DG, CA1, and primary somatosensory cortex in P1 mice. The experimenter was blinded to genotype during quantification.

2.5. Western Blot analysis

Whole brain was dissected from 5 month old WT, *Adgrb1*$^{+/-}$, and Adgrb*1*$^{-/-}$ littermates, and the left hemisphere was used for western blot. Tissue extracts were prepared in RIPA buffer (89901, Thermo Fischer) containing protease and phosphatase inhibitor mix (1861280, Thermo Fischer), and total protein was quantified using the BCA protein assay. Laemmli sample buffer (1610747, Bio-Rad) was added after the BCA protein assay. Protein samples (75 μg) were loaded without boiling on a 10% SDS-PAGE gel, resolved at 100 V/cm for 2.5 h, and transferred to a PVDF membrane (1620177, Bio-Rad). Membranes were blocked with 5% milk and incubated overnight at 4 °C with an anti C-terminal BAI1 antibody (1:1000, AP8170a, Abcepta; epitope: amino acids 1537–1567), followed by an anti-Rabbit HRP-conjugated secondary antibody (1:5000; 31460, Thermo Fischer). The intensity of the Bai1 band was quantified using ImageJ (NIH) as previously described (Zhu et al., 2018) (n = 3/genotype).

2.6. Behavioral analyses

Behavioral analyses were performed on 3–5 month old male *Adgrb1*$^{-/-}$, *Adgrb1*$^{+/-}$, and WT littermates. All behavioral assessments were videotaped and scored using the ANY-Maze Video Tracking System (Stoelting Co.) by an experimenter blinded to genotype. Behavioral analyses were conducted in two cohorts of mice. Cohort 1 underwent novel object recognition followed by three-chamber social interaction one week later. Behavioral tests were conducted in Cohort 2 with one week between tasks: open field, novel cage, nestlet shredding, and buried food test.

2.6.1. Open field and novel object recognition

Open field and novel object recognition were performed as previously described (Dutton et al., 2017; Sawyer et al., 2016; Wong et al., 2021a; Wong et al., 2018). The apparatus consisted of an arena with opaque Plexiglas walls (60 cm × 60 cm × 60 cm). The center zone was a 30 cm × 30 cm area in the center of the chamber. For open field analysis, each mouse was placed in the empty arena and allowed to explore for 10 min. Locomotor activity, total distance traveled, average speed, and the time spent in the center zone were scored (n = 13/genotype). For novel object recognition, open field was performed on day 1. On days 2 and 3, two identical objects (cube or sphere) were placed in the center of the arena, and each mouse explored the arena for 10 min. On day 4, one of

the objects was replaced with a novel object (cube was replaced with the sphere or *vice versa*). The objects and the location of the novel *versus* familiar object were counterbalanced. The time spent exploring each object was used to calculate a discrimination ratio (time exploring the novel object/ (time exploring the novel object + time exploring the familiar object)) (n = 7–8/genotype).

2.6.2. Three-chamber social interaction

Sociability and social discrimination were examined using the three-chamber social interaction paradigm (Dutton et al., 2017; Sawyer et al., 2016; Wong et al., 2021b). A partition separated each chamber (20 cm × 40 cm × 20 cm) with an opening to allow the mouse to move freely between them. The experiment consisted of three 10-min sessions. The test mouse was first placed in the center chamber, with an empty cylindrical wire cage in the left and right chambers, and the mouse was allowed to freely explore for 10 min. In the second 10-min session, an age- and sex-matched C57BL/6J mouse (stranger) was placed under one of the wire cages while the wire cage on the opposite side remained empty (object). The test mouse was again placed in the center chamber and allowed to explore freely. Time interacting with the 'stranger' mouse *vs.* the empty cage was calculated as a measure of 'sociability'. For the third 10-min session, a second age- and sex-matched C57BL/6J mouse (novel mouse) was placed under the previously empty wire cage. The test mouse was again placed in the center chamber and allowed to explore freely. Time interacting with either the first (now 'familiar') mouse from the second session or the novel mouse introduced in the third session was calculated as a measure of 'social discrimination' (n = 7–8/genotype).

2.6.3. Novel cage

Each mouse was placed into a novel standard mouse cage (33 cm × 18 cm × 15 cm) and observed for stereotyped behaviors for 10 min. The time spent grooming, digging, rearing, and circling was recorded (n = 13/genotype).

2.6.4. Nestlet shredding

Nesting behavior was performed as previously described (Lustberg et al., 2020). Each mouse was placed into a novel standard mouse cage with a cotton nestlet square (5 cm × 5 cm, approximately 3 g). Nestlets were weighed before the experiment to calculate the percent shredded at the end of the task. Mice were left undisturbed between 1 pm and 3 pm, after which they were returned to their home cages. The weight of the remaining non-shredded nestlet material was recorded (n = 13/genotype).

2.6.5. Buried food test

Olfactory function was examined using the buried food test as previously described (Yang and Crawley, 2009). Two days prior to assessment of olfactory function, chocolate-flavored pellets (F05472–1, Bio-Serv) were introduced into the home cage to habituate animals to the novel but highly palatable stimulus. Twenty-four hours prior to behavioral testing, all standard mouse chow and chocolate pellets were removed from the home cage. Mice were tested in the same room in which they were housed. On test day, chocolate pellets were placed in a randomly-selected corner of a clean mouse cage and buried under 3 cm of standard bedding. The latency for the mouse to find and eat (grasp and bite) the chocolate pellets was recorded. Mice that did not feed within 15 min were assigned a maximum feeding latency score of 900 s (n = 13/genotype).

2.7. Seizure induction

Susceptibility to induced seizures was tested in 3–5 month old male and female *Adgrb1*$^{-/-}$, *Adgrb1*$^{+/-}$, and WT littermates.

2.7.1. 6 Hz-induced seizures

6 Hz psychomotor seizures were induced as previously described (Giddens et al., 2017; Shapiro et al., 2021; Wong et al., 2016; Wong et al., 2021b). A topical analgesic was applied to the cornea (0.5% tetracaine hydrochloride) before stimulation. Corneal electrical stimulation (6 Hz, 3 s, 17 mA for male and 13 mA for female) was applied through a constant current device (ECT Unit 57800, Ugo Basile), and the mouse was moved immediately into a clean cage for behavioral seizure observation. Resulting seizures were scored on a modified Racine scale: RS0 = no abnormal behavior; RS1 = immobile ≥3 s, RS2 = forelimb clonus, paw waving, RS3 = rearing and falling (n = 8–18/group).

2.7.2. Flurothyl-induced seizures

Seizure induction using flurothyl was performed as previously described (Martin et al., 2007; Shapiro et al., 2021; Shapiro et al., 2019; Wong et al., 2021a). Each mouse was placed in a plexiglass chamber (34 cm × 20 cm × 15 cm and exposed to flurothyl (bis[2,2,2-trifluoroethyl] ether, 287571-5G, Sigma-Aldrich) at a rate of 20 μL/min. Latencies to the first myoclonic jerk (MJ) and generalized tonic-clonic seizure (GTCS) were recorded (n = 8–11/group).

2.8. Statistical analysis

Prism v8.1.2 software (GraphPad) was used for statistical analyses. A 2-way ANOVA followed by Sidak's multiple comparisons test was used to compare the bodyweight of each genotype at the different time points of the growth curve, the time spent interacting with the stranger mouse and novel mouse, total entries into each side chamber during the three-chamber social interaction task, and brain/body weight measurements. For novel object recognition, a one-sample t-test was used to compare the time spent with the novel object against 50% chance. A 1-way ANOVA followed by Tukey's multiple comparisons test was used to analyze the total distance traveled, speed, total time spent in the center of the open field, the latency to the MJ and GTCS during flurothyl seizure induction, the amount of nestlet shredded, the latency to grasp and bite the chocolate pellets in the buried food test, latencies to the first interactions in the three-chamber social interaction task, and immunofluorescence data. For the 6 Hz seizure induction paradigm, an unpaired nonparametric Mann-Whitney U test was used to compare Racine scores between each genotype. Male and female mice were analyzed separately unless stated. All results are presented as mean ± SEM and a p-value ≤0.05 was considered significant.

3. Results

3.1. *Adgrb1*$^{-/-}$ mice show delayed growth and reduced brain weight

Western blot analysis showed that *Adgrb1*$^{-/-}$ mice lack full length Bai1, and *Adgrb1*$^{+/-}$ mutants express approximately 50% of WT levels (Supplementary Fig. 1A-B). We next examined the developmental profile of *Adgrb1* mutants. We observed that *Adgrb1*$^{-/-}$ mice weighed significantly less than their WT littermates beginning at P15 for males (p = 0.0097) (Supplementary Fig. 2A) and P9 for females (p = 0.0112) (Supplementary Fig. 2B); however, by approximately P37, the body weights of *Adgrb1*$^{-/-}$ mice were comparable to same-sex WT littermates. In contrast, there were no significant differences in average body weights between *Adgrb1*$^{+/-}$ and WT littermates at any age.

As Bai1 is highly expressed in the brain, we next focused on brain development. We compared brain and body weights of male and female mice between each genotype at three time points: P1, 3 weeks, and 2–3 months (Fig. 1). At P1, no significant differences were observed in either brain (p = 0.3326) or body weight (p = 0.60) (Fig. 1A-B). However, at 3 weeks of age, average brain weights of *Adgrb1*$^{-/-}$ mice of both sexes were significantly less than sex-matched *Adgrb1*$^{+/-}$ and WT littermates

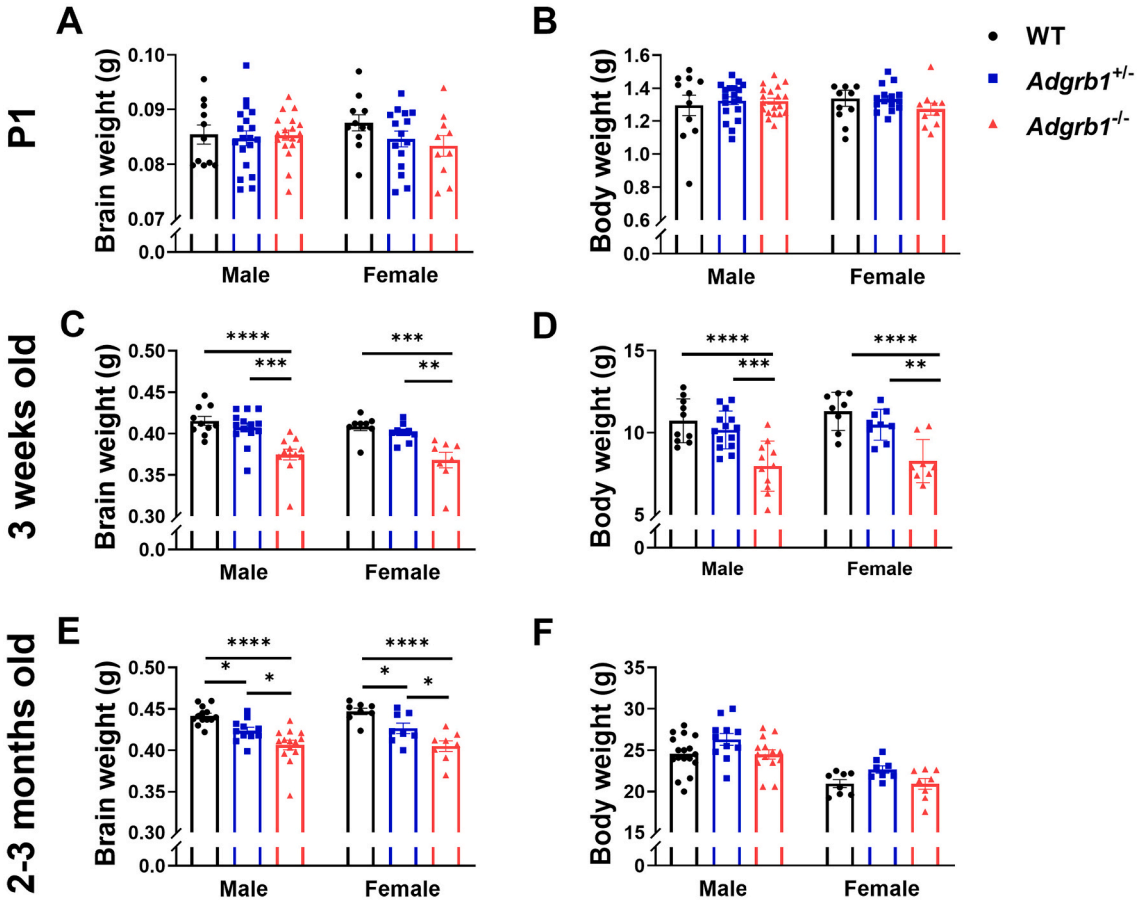

Fig. 1. *Adgrb1*$^{-/-}$ mice exhibit reduced brain and body weight. (A-B) Male and female *Adgrb1*$^{-/-}$ mice (P1) had comparable (A) brain and (B) body weights. Male: WT, $n = 11$; *Adgrb1*$^{+/-}$, $n = 19$; *Adgrb1*$^{-/-}$, n = 19; Female: WT, $n = 10$; *Adgrb1*$^{+/-}$, $n = 15$; *Adgrb1*$^{-/-}$, $n = 10$. (C-D) Male and female *Adgrb1*$^{-/-}$ mice (3 weeks old) had lower average (C) brain and (D) body weights compared to same-sex *Adgrb1*$^{+/-}$ mutants and WT littermates. Male: WT, n = 10; *Adgrb1*$^{+/-}$, $n = 14$; *Adgrb1*$^{-/-}$, $n = 12$; Female: WT, $n = 8$; *Adgrb1*$^{+/-}$, $n = 9$; *Adgrb1*$^{-/-}$, $n = 8$. (E) Male and female *Adgrb1*$^{-/-}$ and *Adgrb1*$^{+/-}$ mice (2–3 months old) had lower average brain weights compared to WT littermates. (F) Body weights were comparable in 2–3 month old mice across all three genotypes. Male: WT, n = 14; *Adgrb1*$^{+/-}$, n = 11; *Adgrb1*$^{-/-}$, n = 14; Female: WT, n = 8; *Adgrb1*$^{+/-}$, n = 8; *Adgrb1*$^{-/-}$, $n = 9$. Mean ± SEM. *$p < 0.05$, **$p < 0.01$, ***$p < 0.001$, ****$p < 0.0001$.

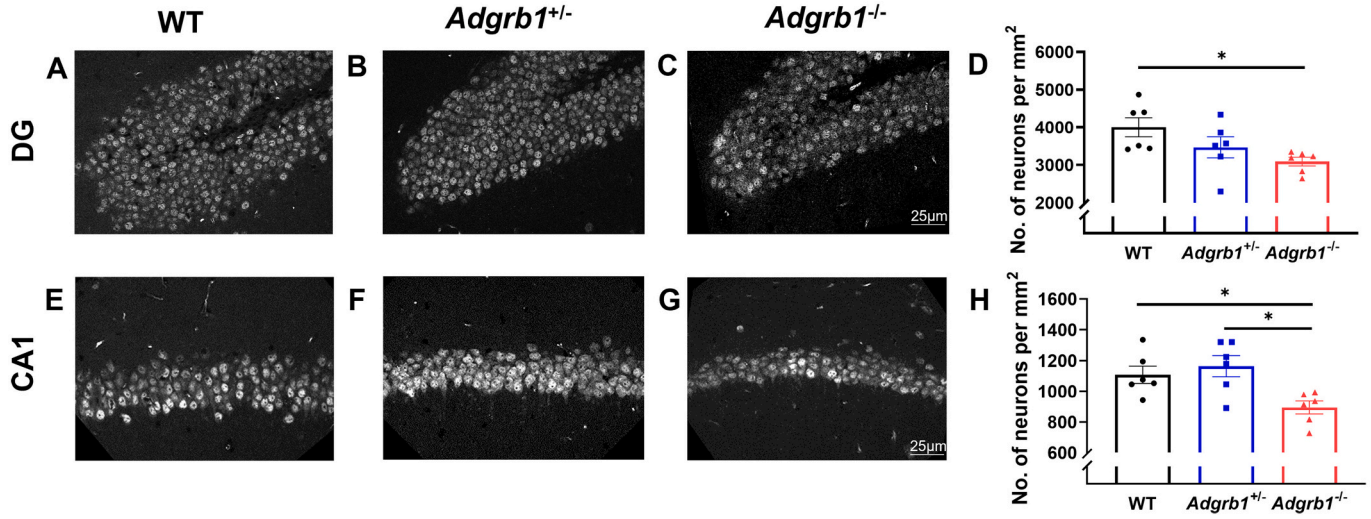

Fig. 2. Reduced neuron density in 2–3 month old *Adgrb1*$^{-/-}$ mice. Representative images of NeuN positive cells in the (A-C) DG and (E-G) CA1 region. *Adgrb1*$^{-/-}$ mice had significantly lower neuron density in the (D) DG and (H) CA1 than *Adgrb1*$^{+/-}$ and WT littermates. WT, $n = 6$; *Adgrb1*$^{+/-}$, n = 6; *Adgrb1*$^{-/-}$, $n = 6$. Mean ± SEM. *$p < 0.05$.

($p < 0.001$) (Fig. 1C). The average body weight of *Adgrb1*$^{-/-}$ mice was also significantly less than sex-matched *Adgrb1*$^{+/-}$ mice and WT littermates ($p = 0.0107$) (Fig. 1D). At 2–3 months of age, no significant differences in average body weights between same-sex mice across all three genotypes were found ($p = 0.998$) (Fig. 1F); however, average brain weights of *Adgrb1*$^{-/-}$ mice of both sexes were significantly less than same-sex *Adgrb1*$^{+/-}$ mice and WT littermates ($p < 0.0001$) (Fig. 1E). In contrast to the other time points, at 2–3 months of age, the average brain weight of *Adgrb1*$^{+/-}$ mice was significantly lower than same-sex WT littermates ($p < 0.05$) (Fig. 1E).

3.2. 2–3 month old *Adgrb1*$^{-/-}$ mice exhibit reduced neuron density in the dentate gyrus and CA1

Since brain weight was lower in 2–3 month old *Adgrb1*$^{-/-}$ mice, we next examined whether brain morphology was altered. We focused on the hippocampus since *Adgrb1*$^{-/-}$ mice were previously shown to exhibit altered hippocampal LTP and LTD, and deficits in hippocampal dependent spatial memory (Zhu et al., 2015). We quantified neuron density in 2–3 month old male mice of each genotype in two hippocampal regions: the DG and CA1. *Adgrb1*$^{-/-}$ male mice displayed significantly lower neuron density in both the DG ($p = 0.0402$) (Fig. 2A-D) and CA1 ($p = 0.0103$) (Fig. 2E-H) compared to WT littermates. We also compared the levels of GFAP (astrocyte marker) and IBA1 (microglia marker) expression in the DG and CA1 between male mice of each genotype (2–3 months old), and observed no significant differences ($p > 0.05$) (Supplementary Fig. 3).

3.3. *Adgrb1*$^{-/-}$ mice exhibit more CC3+ cells in the hippocampal CA1 and primary somatosensory cortex during early postnatal development

To determine whether the reduced neuron density observed in *Adgrb1*$^{-/-}$ mice was associated with a higher level of apoptosis, we used the cleaved caspase-3 antibody (Porter and Janicke, 1999) to compare apoptosis levels in all three genotypes at P1, 3 weeks, and 2–3 months of age. As expected, the number of cleaved caspase-3-positive (CC3+) cells was higher in P1 mice compared to 3 week old and 2–3 month old mice due to the greater level of programmed cell death (PCD) during early neurodevelopment (Yamaguchi and Miura, 2015). At P1, comparable numbers of CC3+ cells were observed in the DG of *Adgrb1*$^{-/-}$ mice and WT littermates ($p = 0.6801$) (Fig. 3A-D); however, we observed a significantly greater number of CC3+ cells in the CA1 region of *Adgrb1*$^{-/-}$ mice ($p = 0.0186$) (Fig. 3E-H). No significant differences were detected between *Adgrb1*$^{+/-}$ mice and WT littermates. We also examined CC3+ cells in the primary somatosensory cortex, a region in which Bai1 is also highly expressed (Sokolowski et al., 2011). Similarly, we observed a greater numbers of CC3+ cells in the somatosensory cortex of P1 *Adgrb1*$^{-/-}$ mice compared to WT littermates ($p = 0.023$) (Supplementary Fig. 4). Comparable numbers of CC3+ cells were observed in the CA1, DG, and primary somatosensory cortex of 3 week old and 2–3 month old mice of each genotype (Supplementary Fig. 5).

3.4. *Adgrb1*$^{-/-}$ mice exhibit deficits in social behavior and learning and memory

We used the three-chamber social interaction paradigm to examine sociability and social discrimination as BAI1 interacts with the autism relevant proteins, NLG1 and IRSp53, and mice lacking Nlg1 or Irsp53 show altered social behavior (Blundell et al., 2010; Chung et al., 2015). During the sociability component, WT littermates and *Adgrb1*$^{+/-}$ mice spent significantly more time exploring the stranger mouse than the empty cage (WT, $p = 0.0008$; *Adgrb1*$^{+/-}$, $p = 0.0099$). In contrast, *Adgrb1*$^{-/-}$ mice did not discriminate between the stranger mouse and empty cage ($p = 0.6627$), suggesting a deficit in sociability (Fig. 4A). When presented with the choice between interacting with a novel or familiar mouse, WT littermates showed a significant preference for the novel mouse ($p = 0.0097$). In contrast, *Adgrb1*$^{+/-}$ and *Adgrb1*$^{-/-}$ mice did not show a statistically significant preference for the novel mouse (*Adgrb1*$^{+/-}$, $p = 0.0984$; *Adgrb1*$^{-/-}$, $p = 0.7451$), suggesting a deficit in social discrimination (Fig. 4B). There were no differences in total entries into each side chamber or the latencies to the first interaction with the stranger mouse or the novel mouse in the 'sociability' and 'social discrimination' components of the task, respectively (Supplementary Fig. 6). The similar performance of mice of all three genotypes in the buried food test (Fig. 4C) demonstrates that the observed impairment in social interaction is unlikely to be due to olfactory dysfunction.

In addition to abnormalities in social behavior, deficits in learning and memory have been described in patients and animal models of ASD (Pasciuto et al., 2015; Silverman et al., 2010). Therefore, we used the novel object recognition task to examine long-term recognition memory. WT littermates and *Adgrb1*$^{+/-}$ mice spent significantly more time exploring the novel object compared to 50% chance (WT, $p < 0.001$;

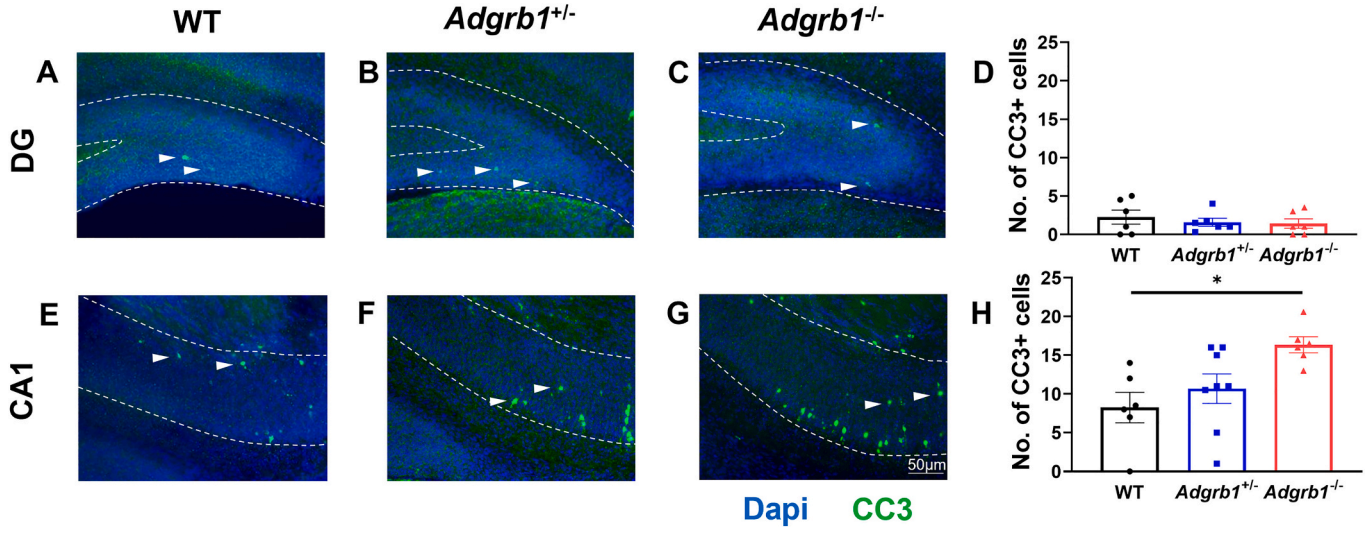

Fig. 3. P1 *Adgrb1*$^{-/-}$ mice have more CC3+ cells in the CA1. (A-C) Representative images of CC3+ cells in the DG. (D) Comparable numbers of CC3+ cells in the DG were observed across all three genotypes. (E-G) Representative images of CC3+ cells in the CA1. (H) *Adgrb1*$^{-/-}$ mice had more CC3+ cells in the CA1 than WT littermates. Dashed lines indicate the boundaries of the DG and CA1 regions. Examples of CC3+ cells are indicated with arrows. WT, n = 6; *Adgrb1*$^{+/-}$, n = 6; *Adgrb1*$^{-/-}$, n = 6. Mean ± SEM. *$p < 0.05$.

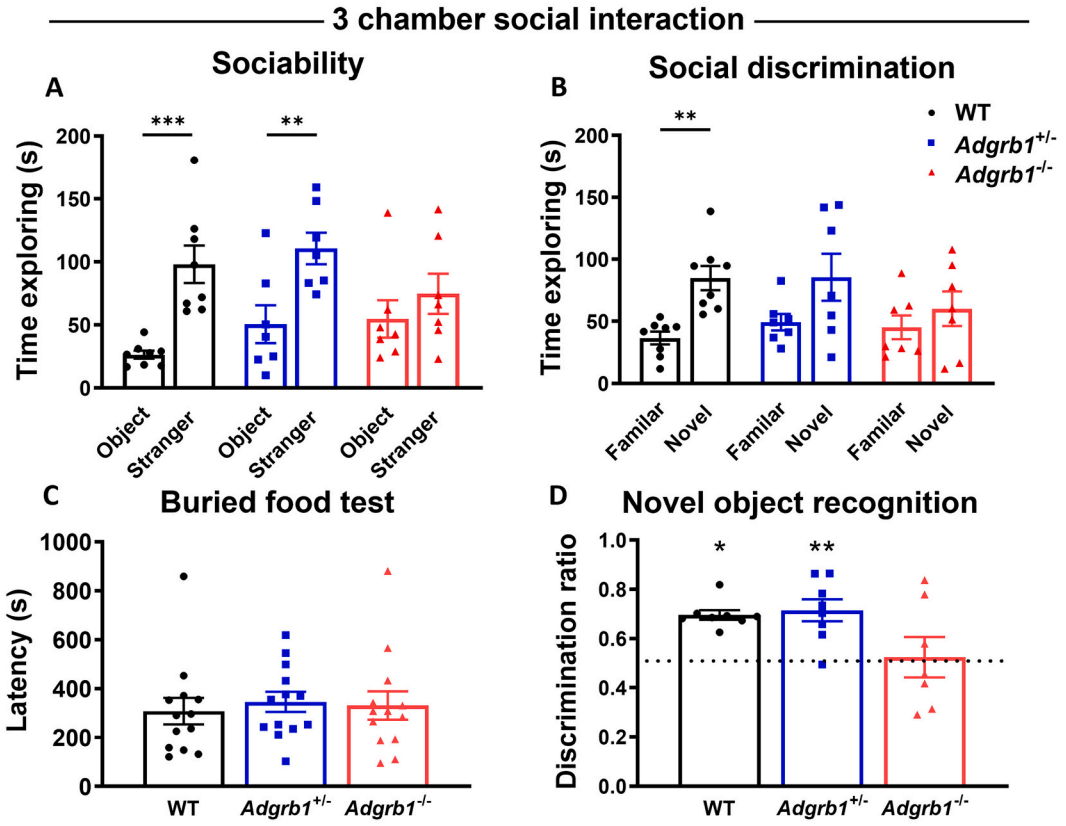

Fig. 4. Male *Adgrb1*$^{-/-}$ mice exhibit deficits in sociability, social discrimination, and recognition memory. (A) *Adgrb1*$^{-/-}$ mice did not significantly discriminate between a stranger mouse and an empty cage, demonstrating a sociability deficit. (B) *Adgrb1*$^{+/-}$ and *Adgrb1*$^{-/-}$ mutants did not exhibit a significant preference for a novel *vs.* a familiar mouse, indicating a deficit in social discrimination. WT, $n = 8$; *Adgrb1*$^{+/-}$, n = 8; *Adgrb1*$^{-/-}$, $n = 7$. (C) The latency to find buried food was comparable across genotypes. WT, $n = 13$; *Adgrb1*$^{+/-}$, n = 13; *Adgrb1*$^{-/-}$, n = 13. (D) *Adgrb1*$^{-/-}$ mice did not discriminate between the novel and familiar object, suggesting a deficit in long-term recognition memory. WT, n = 8; *Adgrb1*$^{+/-}$, n = 8; *Adgrb1*$^{-/-}$, n = 7. Mean ± SEM. *$p < 0.05$, **$p < 0.01$, ***$p < 0.001$.

Adgrb1$^{+/-}$, $p = 0.0019$) (Fig. 4D). In contrast, *Adgrb1*$^{-/-}$ mice did not show a significant preference for the novel object ($p = 0.7765$), suggesting a deficit in long-term recognition memory.

We also subjected the mice to the open field paradigm to examine locomotor activity and anxiety-like behavior. Distance traveled ($p = 0.187$) (Supplementary Fig. 7A) and average speed ($p = 0.1865$) (Supplementary Fig. 7B) were found to be comparable between the three genotypes. *Adgrb1*$^{-/-}$ mice spent more time than WT littermates in the center of the open field ($p = 0.012$), suggesting that loss of full length Bai1 is not associated with increased anxiety-like behavior (Supplementary Fig. 7C). Lastly, we examined nesting behavior (Supplementary Fig. 7D) and stereotypical behaviors (Supplementary Fig. 7E) and found that all three genotypes performed similarly ($p = 0.294$ and 0.328, respectively).

3.5. *Adgrb1*$^{-/-}$ mice are susceptible to induced seizures

Along with social deficits, many mouse models of ASD exhibit an increased vulnerability to seizures, an observation that is consistent with clinical observations that epilepsy is often comorbid with ASD (Ghacibeh and Fields, 2015; Hughes and Melyn, 2005). Therefore, we explored whether *Adgrb1* mutants might exhibit alterations in seizure susceptibility. In the 6 Hz paradigm, seizures were observed in all *Adgrb1*$^{-/-}$ mice (male: 3 RS1, 7 RS2; $p = 0.0185$, female: 6 RS2, 2 RS3; $p = 0.0039$) (Fig. 5A and D). In contrast, only 25% and 33% of male and female WT littermates seized, respectively (male: 6 RS0, 2 RS2; female: 6 RS0, 3 RS2). Additionally, when exposed to the proconvulsant flurothyl, *Adgrb1*$^{-/-}$ mutants displayed shorter average latencies to the first myoclonic jerk (MJ) (male, $p < 0.0001$; female, $p = 0.0002$) (Fig. 5B and E) and generalized tonic-clonic seizure (GTCS) (male, $p = 0.0004$; female, $p = 0.0014$) when compared to same-sex WT littermates (Fig. 5C and F). In contrast, there were no differences in the average latency to the MJ or GTCS between same-sex heterozygous mutants and WT littermates.

4. Discussion

In the current study, we identified a wide range of phenotypes, including delayed growth, reduced brain weight, higher number of CC3+ cells, deficits in social behavior, and increased seizure susceptibility in mice lacking full length Bai1. These observations expand the clinical features that could be potentially associated with BAI1 dysfunction.

We found that 3 week old *Adgrb1*$^{-/-}$ mice weighed significantly less than *Adgrb1*$^{+/-}$ and WT littermates; however, body weight was comparable between genotypes at 2–3 months of age. Lower body weight during early development has been previously reported for several mouse models of autism (Portmann et al., 2014; Yang et al., 2016). It is possible that competition with the WT littermates prior to weaning could have reduced milk intake in the mutants, thereby contributing to the slower initial weight gain. In contrast, at both the 3 week and 2–3 month time points, the average brain weight of *Adgrb1*$^{-/-}$ mutants was significantly less than WT littermates. Thus, the lower brain weight in *Adgrb1*$^{-/-}$ mutants was not simply due to the overall smaller size of the mutant mice. Consistent with the lower brain weights, we observed reduced neuron density in the DG and CA1 regions of 2–3 month old *Adgrb1*$^{-/-}$ mice. Since Bai1 is known to mediate the clearance of apoptotic cells (Mazaheri et al., 2014; Sokolowski et al., 2011), we

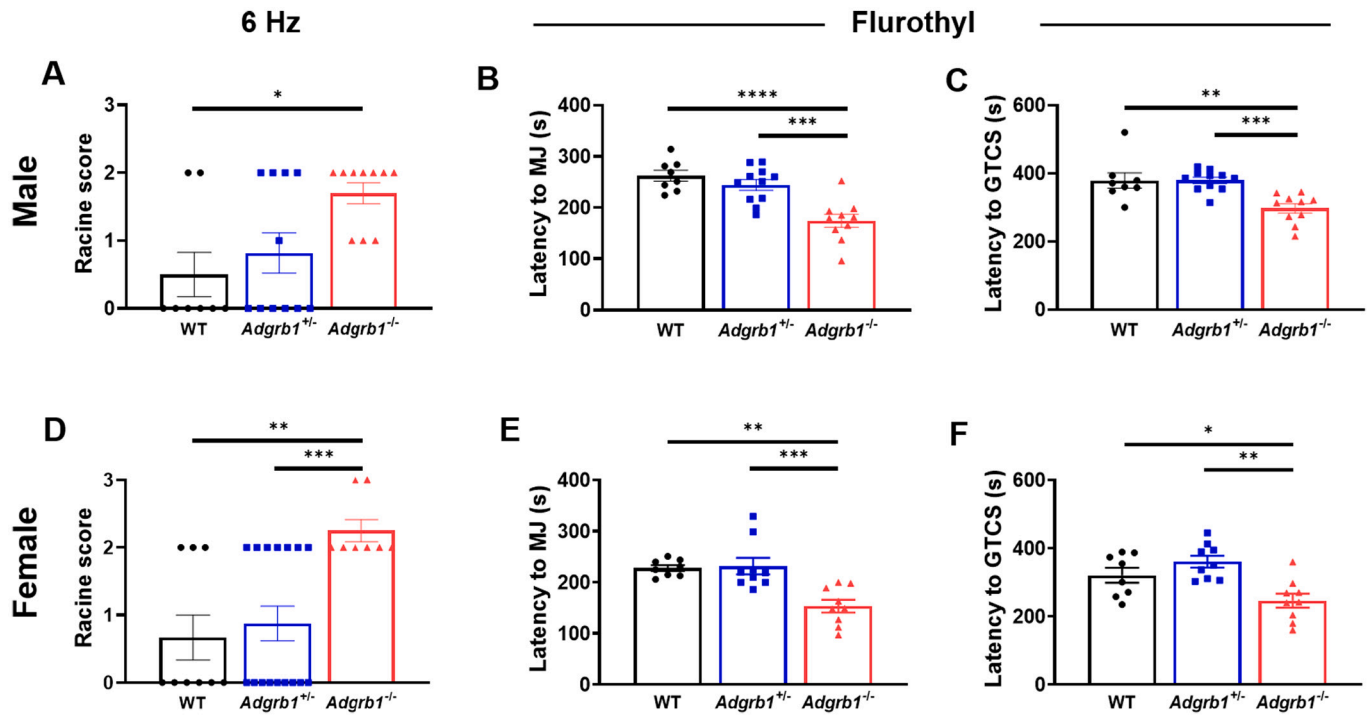

Fig. 5. *Adgrb1*$^{-/-}$ mice are susceptible to induced seizures. (A and D) Male and female *Adgrb1*$^{-/-}$ mice were more susceptible to 6 Hz seizures when compared to same-sex *Adgrb1*$^{+/-}$ and WT littermates. Male: WT, $n = 8$; *Adgrb1*$^{+/-}$, $n = 11$; *Adgrb1*$^{-/-}$, $n = 10$; Female: WT, $n = 9$; *Adgrb1*$^{+/-}$, $n = 18$; *Adgrb1*$^{-/-}$, $n = 8$. (B and E) Male and female *Adgrb1*$^{-/-}$ mutants exhibited shorter latencies to the first flurothyl-induced myoclonic jerk (MJ) and (C and F) generalized tonic-clonic seizure (GTCS) compared to same-sex *Adgrb1*$^{+/-}$ and WT littermates. Male: WT, n = 8; *Adgrb1*$^{+/-}$, n = 11; *Adgrb1*$^{-/-}$, n = 10, Female: WT, n = 8; *Adgrb1*$^{+/-}$, n = 9; *Adgrb1*$^{-/-}$, $n = 9$. Mean ± SEM. *$p < 0.05$, **$p < 0.01$, ***$p < 0.001$, ****$p < 0.0001$.

speculated that the absence of full-length Bai1 during early brain development may result in increased levels of uncleared apoptotic cells. In turn, this could contribute to secondary necrosis, neuron loss, and lower brain weight (Elliott and Ravichandran, 2010; Glass et al., 2010). In support of this prediction, we observed increased CC3+ cells in the CA1 region and somatosensory cortex of P1 *Adgrb1*$^{-/-}$ mice. Interestingly, the number of CC3+ cells in these regions was comparable between the three genotypes at the 3 week and 2–3 month time points, suggesting that Bai1 might play a greater role in the clearance of apoptotic cells early in brain development, a period that has the highest levels of apoptosis due to programmed cell death (Ahern et al., 2013; Yamaguchi and Miura, 2015).

While we observed reduced neuron density in both CA1 and DG of 2–3 month old *Adgrb1*$^{-/-}$ mice, similar numbers of CC3+ cells were detected in the DG of P1 *Adgrb1*$^{-/-}$ mice and WT littermates. This suggests reduced clearance of apoptotic cells during early development is unlikely to be solely responsible for the observation of reduced neuron density. Thus, additional studies will be required to fully resolve the underlying mechanisms.

Sequence analysis of ASD patients recently identified several *de novo* BAI1 variants (Satterstrom et al., 2020), suggesting that BAI1 might play a role in ASD. BAI1 interacts with autism-associated proteins, such as NLG1 and BAIAP2/IRSp53 (Nakanishi et al., 2017; Shiratsuchi et al., 1998; Toma et al., 2011; Tu et al., 2018). *Nlg1*$^{-/-}$ and *Irsp53*$^{-/-}$ mice show abnormal social behavior, memory deficits, and altered synaptic plasticity (Blundell et al., 2010; Chung et al., 2015; Kim et al., 2009). However, while the phenotypes of *Adgrb1*$^{-/-}$ mutants overlap with *Nlg1*$^{-/-}$ and *Irsp53*$^{-/-}$ mice, the mechanisms underlying the observed phenotypes might not be identical. Lack of full-length Bai1 leads to rapid degradation of Psd-95 due to the activation of the E3 ubiquitin ligase Mdm2 (Zhu et al., 2015), and mice lacking Psd-95 similarly demonstrate sociability and memory deficits (Coley and Gao, 2019; Migaud et al., 1998). However, no changes in Psd-95 protein levels were reported in *Irsp53*$^{-/-}$ and *Nlg1*$^{-/-}$ mice (Blundell et al., 2010; Kim et al., 2009), indicating other pathways might exist that cause the similar deficits observed in *Nlg1*$^{-/-}$ and *Irsp53*$^{-/-}$ mice.

In addition to the memory and social behavior deficits observed in the *Adgrb1* mutants, we also found that these mice are more seizure susceptible. While the mechanistic basis for this observation is currently unknown, it may be due, in part, to disrupted protein-protein interactions. For example, BAI1 interacts with BAI1 associated protein 3 (BAIAP3), which mediates endosome fusion within the trans-Golgi network (Zhang et al., 2017). BAIAP3 can modulate GABAergic neuronal firing (Wojcik et al., 2013), and *Baiap3*$^{-/-}$ mice also exhibit increased seizure susceptibility (Wojcik et al., 2013). Furthermore, *Adgrb1* mutants exhibit enhanced NMDA mediated LTP, which can also be an underlying cause of increased seizure susceptibility (Kapur, 2018).

While the alterations in sociability, seizure susceptibility, and body weight were only observed in homozygous *Adgrb1*$^{-/-}$ mutants, brain weight was reduced in both the *Adgrb1*$^{+/-}$ and *Adgrb1*$^{-/-}$ mutants. These observations demonstrate that Bai1 haploinsufficiency can influence biological processes and that some disease phenotypes associated with Bai1 dysfunction may be affected by gene dosage. The current study reveals previously undescribed roles for BAI1 in regulating social behavior, seizure vulnerability, and CNS development, thus implicating BAI1 in a range of clinically challenging neurological disorders, including ASD and epilepsy.

Acknowledgements

We would like to thank Laura Fox-Goharioon of the Emory Integrated Cellular Imaging Core, Daniel Lustberg for assisting with the buried food test, and the Emory Neuroscience NINDS Core Facilities for support and assistance with confocal imaging. We also thank Dr. Deborah Cook for editorial assistance.

Funding sources

This work was supported by the National Institutes of Health (EGVM, CA096236 and NS117666), Emory University Integrated Cellular Imaging Microscopy Core of the Emory Neuroscience NINDS Core Facilities grant (5P30NS055077), and the Emory Brain Health Center (EGVM, RAH, AE). The content is solely the responsibility of the authors and does not necessarily reflect the official views of the National Institutes of Health.

Disclosure of conflict of interests

The authors declare no conflict of interest.

Appendix A. Supplementary data

Supplementary data to this article can be found online at https://doi.org/10.1016/j.expneurol.2022.113994.

References

Ahern, T.H., Krug, S., Carr, A.V., Murray, E.K., Fitzpatrick, E., Bengston, L., McCutcheon, J., De Vries, G.J., Forger, N.G., 2013. Cell death atlas of the postnatal mouse ventral forebrain and hypothalamus: effects of age and sex. J. Comp. Neurol. 521, 2551–2569. https://doi.org/10.1002/cne.23298.

Amiet, C., Gourfinkel-An, I., Bouzamondo, A., Tordjman, S., Baulac, M., Lechat, P., Mottron, L., Cohen, D., 2008. Epilepsy in autism is associated with intellectual disability and gender: evidence from a meta-analysis. Biol. Psychiatry 64, 577–582. https://doi.org/10.1016/j.biopsych.2008.04.030.

Blundell, J., Blaiss, C.A., Etherton, M.R., Espinosa, F., Tabuchi, K., Walz, C., Bolliger, M. F., Sudhof, T.C., Powell, C.M., 2010. Neuroligin-1 deletion results in impaired spatial memory and increased repetitive behavior. J. Neurosci. 30, 2115–2129. https://doi.org/10.1523/JNEUROSCI.4517-09.2010.

Chalermpalanupap, T., Schroeder, J.P., Rorabaugh, J.M., Liles, L.C., Lah, J.J., Levey, A.I., Weinshenker, D., 2018. Locus Coeruleus ablation exacerbates cognitive deficits, neuropathology, and lethality in P301S tau transgenic mice. J. Neurosci. 38, 74–92. https://doi.org/10.1523/JNEUROSCI.1483-17.2017.

Cheng, D., Hoogenraad, C.C., Rush, J., Ramm, E., Schlager, M.A., Duong, D.M., Xu, P., Wijayawardana, S.R., Hanfelt, J., Nakagawa, T., Sheng, M., Peng, J., 2006. Relative and absolute quantification of postsynaptic density proteome isolated from rat forebrain and cerebellum. Mol. Cell. Proteomics 5, 1158–1170. https://doi.org/10.1074/mcp.D500009-MCP200.

Chung, W., Choi, S.Y., Lee, E., Park, H., Kang, J., Park, H., Choi, Y., Lee, D., Park, S.G., Kim, R., Cho, Y.S., Choi, J., Kim, M.H., Lee, J.W., Lee, S., Rhim, I., Jung, M.W., Kim, D., Bae, Y.C., Kim, E., 2015. Social deficits in IRSp53 mutant mice improved by NMDAR and mGluR5 suppression. Nat. Neurosci. 18, 435–443. https://doi.org/10.1038/nn.3927.

Coley, A.A., Gao, W.J., 2018. PSD95: A synaptic protein implicated in schizophrenia or autism? Prog. Neuro-Psychopharmacol. Biol. Psychiatry 82, 187–194. https://doi.org/10.1016/j.pnpbp.2017.11.016.

Coley, A.A., Gao, W.J., 2019. PSD-95 deficiency disrupts PFC-associated function and behavior during neurodevelopment. Sci. Rep. 9, 9486. https://doi.org/10.1038/s41598-019-45971-w.

Cork, S.M., Van Meir, E.G., 2011. Emerging roles for the BAI1 protein family in the regulation of phagocytosis, synaptogenesis, neurovasculature, and tumor development. J. Mol. Med. (Berl). 89, 743–752. https://doi.org/10.1007/s00109-011-0759-x.

Cork, S.M., Kaur, B., Devi, N.S., Cooper, L., Saltz, J.H., Sandberg, E.M., Kaluz, S., Van Meir, E.G., 2012. A proprotein convertase/MMP-14 proteolytic cascade releases a novel 40 kDa vasculostatin from tumor suppressor BAI1. Oncogene. 31, 5144–5152. https://doi.org/10.1038/onc.2012.1.

Das, S., Owen, K.A., Ly, K.T., Park, D., Black, S.G., Wilson, J.M., Sifri, C.D., Ravichandran, K.S., Ernst, P.B., Casanova, J.E., 2011. Brain angiogenesis inhibitor 1 (BAI1) is a pattern recognition receptor that mediates macrophage binding and engulfment of gram-negative bacteria. Proc. Natl. Acad. Sci. U. S. A. 108, 2136–2141. https://doi.org/10.1073/pnas.1014775108.

De Rubeis, S., He, X., Goldberg, A.P., Poultney, C.S., Samocha, K., Cicek, A.E., Kou, Y., Liu, L., Fromer, M., Walker, S., Singh, T., Klei, L., Kosmicki, J., Shih-Chen, F., Aleksic, B., Biscaldi, M., Bolton, P.F., Brownfeld, J.M., Cai, J., Campbell, N.G., Carracedo, A., Chahrour, M.H., Chiocchetti, A.G., Coon, H., Crawford, E.L., Curran, S.R., Dawson, G., Duketis, E., Fernandez, B.A., Gallagher, L., Geller, E., Guter, S.J., Hill, R.S., Ionita-Laza, J., Jimenz Gonzalez, P., Kilpinen, H., Klauck, S.M., Kolevzon, A., Lee, I., Lei, I., Lei, J., Lehtimaki, T., Lin, C.F., Ma'ayan, A., Marshall, C. R., McInnes, A.L., Neale, B., Owen, M.J., Ozaki, N., Parellada, M., Parr, J.R., Purcell, S., Puura, K., Rajagopalan, D., Rehnstrom, K., Reichenberg, A., Sabo, A., Sachse, M., Sanders, S.J., Schafer, C., Schulte-Ruther, M., Skuse, D., Stevens, C., Szatmari, P., Tammimies, K., Valladares, O., Voran, A., Li-San, W., Weiss, L.A., Willsey, A.J., Yu, T.W., Yuen, R.K., Cook, E.H., Freitag, C.M., Gill, M., Hultman, C. M., Lehner, T., Palotie, A., Schellenberg, G.D., Sklar, P., State, M.W., Sutcliffe, J.S., Walsh, C.A., Scherer, S.W., Zwick, M.E., Barett, J.C., Cutler, D.J., Roeder, K., Devlin, B., Daly, M.J., Buxbaum, J.D., Study, D. D. D., Homozygosity Mapping Collaborative for, A., Consortium, U. K, 2014. Synaptic, transcriptional and chromatin genes disrupted in autism. Nature. 515, 209–215. https://doi.org/10.1038/nature13772.

Duman, J.G., Tzeng, C.P., Tu, Y.K., Munjal, T., Schwechter, B., Ho, T.S., Tolias, K.F., 2013. The adhesion-GPCR BAI1 regulates synaptogenesis by controlling the recruitment of the Par3/Tiam1 polarity complex to synaptic sites. J. Neurosci. 33, 6964–6978. https://doi.org/10.1523/JNEUROSCI.3978-12.2013.

Duman, J.G., Tu, Y.K., Tolias, K.F., 2016. Emerging roles of BAI adhesion-GPCRs in synapse development and plasticity. Neural. Plast. 2016, 8301737. https://doi.org/10.1155/2016/8301737.

Duman, J.G., Mulherkar, S., Tu, Y.K., Erikson, K.C., Tzeng, C.P., Mavratsas, V.C., Ho, T. S., Tolias, K.F., 2019. The adhesion-GPCR BAI1 shapes dendritic arbors via Bcr-mediated RhoA activation causing late growth arrest. Elife. 8 https://doi.org/10.7554/eLife.47566.

Dutton, S.B.B., Dutt, K., Papale, L.A., Helmers, S., Goldin, A.L., Escayg, A., 2017. Early-life febrile seizures worsen adult phenotypes in Scn1a mutants. Exp. Neurol. 293, 159–171. https://doi.org/10.1016/j.expneurol.2017.03.026.

Elliott, M.R., Ravichandran, K.S., 2010. Clearance of apoptotic cells: implications in health and disease. J. Cell Biol. 189, 1059–1070. https://doi.org/10.1083/jcb.201004096.

Gabis, L., Pomeroy, J., Andriola, M.R., 2005. Autism and epilepsy: cause, consequence, comorbidity, or coincidence? Epilepsy Behav. 7, 652–656. https://doi.org/10.1016/j.yebeh.2005.08.008.

Ghacibeh, G.A., Fields, C., 2015. Interictal epileptiform activity and autism. Epilepsy Behav. 47, 158–162. https://doi.org/10.1016/j.yebeh.2015.02.025.

Giddens, M.M., Wong, J.C., Schroeder, J.P., Farrow, E.G., Smith, B.M., Owino, S., Soden, S.E., Meyer, R.C., Saunders, C., LePichon, J.B., Weinshenker, D., Escayg, A., Hall, R.A., 2017. GPR37L1 modulates seizure susceptibility: evidence from mouse studies and analyses of a human GPR37L1 variant. Neurobiol. Dis. 106, 181–190. https://doi.org/10.1016/j.nbd.2017.07.006.

Glass, C.K., Saijo, K., Winner, B., Marchetto, M.C., Gage, F.H., 2010. Mechanisms underlying inflammation in neurodegeneration. Cell. 140, 918–934. https://doi.org/10.1016/j.cell.2010.02.016.

Hochreiter-Hufford, A.E., Lee, C.S., Kinchen, J.M., Sokolowski, J.D., Arandjelovic, S., Call, J.A., Klibanov, A.L., Yan, Z., Mandell, J.W., Ravichandran, K.S., 2013. Phosphatidylserine receptor BAI1 and apoptotic cells as new promoters of myoblast fusion. Nature. 497, 263–267. https://doi.org/10.1038/nature12135.

Hughes, J.R., Melyn, M., 2005. EEG and seizures in autistic children and adolescents: further findings with therapeutic implications. Clin. EEG Neurosci. 36, 15–20. https://doi.org/10.1177/155005940503600105.

Kapur, J., 2018. Role of NMDA receptors in the pathophysiology and treatment of status epilepticus. Epilepsia Open. 3, 165–168. https://doi.org/10.1002/epi4.12270.

Kaur, B., Cork, S.M., Sandberg, E.M., Devi, N.S., Zhang, Z., Klenotic, P.A., Febbraio, M., Shim, H., Mao, H., Tucker-Burden, C., Silverstein, R.L., Brat, D.J., Olson, J.J., Van Meir, E.G., 2009. Vasculostatin inhibits intracranial glioma growth and negatively regulates in vivo angiogenesis through a CD36-dependent mechanism. Cancer Res. 69, 1212–1220. https://doi.org/10.1158/0008-5472.CAN-08-1166.

Kee, H.J., Ahn, K.Y., Choi, K.C., Won Song, J., Heo, T., Jung, S., Kim, J.K., Bae, C.S., Kim, K.K., 2004. Expression of brain-specific angiogenesis inhibitor 3 (BAI3) in normal brain and implications for BAI3 in ischemia-induced brain angiogenesis and malignant glioma. FEBS Lett. 569, 307–316. https://doi.org/10.1016/j.febslet.2004.06.011.

Kim, M.H., Choi, J., Yang, J., Chung, W., Kim, J.H., Paik, S.K., Kim, K., Han, S., Won, H., Bae, Y.S., Cho, S.H., Seo, J., Bae, Y.C., Choi, S.Y., Kim, E., 2009. Enhanced NMDA receptor-mediated synaptic transmission, enhanced long-term potentiation, and impaired learning and memory in mice lacking IRSp53. J. Neurosci. 29, 1586–1595. https://doi.org/10.1523/JNEUROSCI.4306-08.2009.

Lin, Y.C., Koleske, A.J., 2010. Mechanisms of synapse and dendrite maintenance and their disruption in psychiatric and neurodegenerative disorders. Annu. Rev. Neurosci. 33, 349–378. https://doi.org/10.1146/annurev-neuro-060909-153204.

Lustberg, D., Iannitelli, A.F., Tillage, R.P., Pruitt, M., Liles, L.C., Weinshenker, D., 2020. Central norepinephrine transmission is required for stress-induced repetitive behavior in two rodent models of obsessive-compulsive disorder. Psychopharmacology 237, 1973–1987. https://doi.org/10.1007/s00213-020-05512-0.

Martin, M.S., Tang, B., Papale, L.A., Yu, F.H., Catterall, W.A., Escayg, A., 2007. The voltage-gated sodium channel Scn8a is a genetic modifier of severe myoclonic epilepsy of infancy. Hum. Mol. Genet. 16, 2892–2899. https://doi.org/10.1093/hmg/ddm248.

Mazaheri, F., Breus, O., Durdu, S., Haas, P., Wittbrodt, J., Gilmour, D., Peri, F., 2014. Distinct roles for BAI1 and TIM-4 in the engulfment of dying neurons by microglia. Nat. Commun. 5, 4046. https://doi.org/10.1038/ncomms5046.

Migaud, M., Charlesworth, P., Dempster, M., Webster, L.C., Watabe, A.M., Makhinson, M., He, Y., Ramsay, M.F., Morris, R.G., Morrison, J.H., O'Dell, T.J., Grant, S.G., 1998. Enhanced long-term potentiation and impaired learning in mice with mutant postsynaptic density-95 protein. Nature. 396, 433–439. https://doi.org/10.1038/24790.

Nakanishi, M., Nomura, J., Ji, X., Tamada, K., Arai, T., Takahashi, E., Bucan, M., Takumi, T., 2017. Functional significance of rare neuroligin 1 variants found in autism. PLoS Genet. 13, e1006940 https://doi.org/10.1371/journal.pgen.1006940.

Oda, K., Shiratsuchi, T., Nishimori, H., Inazawa, J., Yoshikawa, H., Taketani, Y., Nakamura, Y., Tokino, T., 1999. Identification of BAIAP2 (BAI-associated protein 2), a novel human homologue of hamster IRSp53, whose SH3 domain interacts with the cytoplasmic domain of BAI1. Cytogenet. Cell Genet. 84, 75–82. https://doi.org/10.1159/000015219.

Park, D., Tosello-Trampont, A.C., Elliott, M.R., Lu, M., Haney, L.B., Ma, Z., Klibanov, A. L., Mandell, J.W., Ravichandran, K.S., 2007. BAI1 is an engulfment receptor for apoptotic cells upstream of the ELMO/Dock180/Rac module. Nature. 450, 430–434. https://doi.org/10.1038/nature06329.

Pasciuto, E., Borrie, S.C., Kanellopoulos, A.K., Santos, A.R., Cappuyns, E., D'Andrea, L., Pacini, L., Bagni, C., 2015. Autism Spectrum disorders: translating human deficits into mouse behavior. Neurobiol. Learn. Mem. 124, 71–87. https://doi.org/10.1016/j.nlm.2015.07.013.

Penzes, P., Cahill, M.E., Jones, K.A., VanLeeuwen, J.E., Woolfrey, K.M., 2011. Dendritic spine pathology in neuropsychiatric disorders. Nat. Neurosci. 14, 285–293. https://doi.org/10.1038/nn.2741.

Porter, A.G., Janicke, R.U., 1999. Emerging roles of caspase-3 in apoptosis. Cell Death Differ. 6, 99–104. https://doi.org/10.1038/sj.cdd.4400476.

Portmann, T., Yang, M., Mao, R., Panagiotakos, G., Ellegood, J., Dolen, G., Bader, P.L., Grueter, B.A., Goold, C., Fisher, E., Clifford, K., Rengarajan, P., Kalikhman, D., Loureiro, D., Saw, N.L., Zhengqui, Z., Miller, M.A., Lerch, J.P., Henkelman, M., Shamloo, M., Malenka, R.C., Crawley, J.N., Dolmetsch, R.E., 2014. Behavioral abnormalities and circuit defects in the basal ganglia of a mouse model of 16p11.2 deletion syndrome. Cell Rep. 7, 1077–1092. https://doi.org/10.1016/j.celrep.2014.03.036.

Purcell, R.H., Hall, R.A., 2018. Adhesion G protein-coupled receptors as drug targets. Annu. Rev. Pharmacol. Toxicol. 58, 429–449. https://doi.org/10.1146/annurev-pharmtox-010617-052933.

Satterstrom, F.K., Kosmicki, J.A., Wang, J., Breen, M.S., De Rubeis, S., An, J.Y., Peng, M., Collins, R., Grove, J., Klei, L., Stevens, C., Reichert, J., Mulhern, M.S., Artomov, M., Gerges, S., Sheppard, B., Xu, X., Bhaduri, A., Norman, U., Brand, H., Schwartz, G., Nguyen, R., Guerrero, E.E., Dias, C., Autism Sequencing, C., I, P.-B. C, Betancur, C., Cook, E.H., Gallagher, L., Gill, M., Sutcliffe, J.S., Thurm, A., Zwick, M.E., Borglum, A.D., State, M.W., Cicek, A.E., Talkowski, M.E., Cutler, D.J., Devlin, B., Sanders, S.J., Roeder, K., Daly, M.J., Buxbaum, J.D., 2020. Large-scale exome sequencing study implicates both developmental and functional changes in the neurobiology of Autism. Cell. 180 (568–584), e23 https://doi.org/10.1016/j.cell.2019.12.036.

Sawyer, N.T., Helvig, A.W., Makinson, C.D., Decker, M.J., Neigh, G.N., Escayg, A., 2016. Scn1a dysfunction alters behavior but not the effect of stress on seizure response. Genes Brain Behav. 15, 335–347. https://doi.org/10.1111/gbb.12281.

Shapiro, L., Wong, J.C., Escayg, A., 2019. Reduced cannabinoid 2 receptor activity increases susceptibility to induced seizures in mice. Epilepsia. 60, 2359–2369. https://doi.org/10.1111/epi.16388.

Shapiro, L., Gado, F., Manera, C., Escayg, A., 2021. Allosteric modulation of the cannabinoid 2 receptor confers seizure resistance in mice. Neuropharmacology. 188, 108448 https://doi.org/10.1016/j.neuropharm.2021.108448.

Shiratsuchi, T., Futamura, M., Oda, K., Nishimori, H., Nakamura, Y., Tokino, T., 1998. Cloning and characterization of BAI-associated protein 1: a PDZ domain-containing protein that interacts with BAI1. Biochem. Biophys. Res. Commun. 247, 597–604. https://doi.org/10.1006/bbrc.1998.8603.

Sierra-Arregui, T., Llorente, J., Gimenez Minguez, P., Tonnesen, J., Penagarikano, O., 2020. Neurobiological mechanisms of Autism spectrum disorder and epilepsy, insights from animal models. Neuroscience. 445, 69–82. https://doi.org/10.1016/j.neuroscience.2020.02.043.

Silverman, J.L., Yang, M., Lord, C., Crawley, J.N., 2010. Behavioural phenotyping assays for mouse models of autism. Nat. Rev. Neurosci. 11, 490–502. https://doi.org/10.1038/nrn2851.

Sokolowski, J.D., Nobles, S.L., Heffron, D.S., Park, D., Ravichandran, K.S., Mandell, J.W., 2011. Brain-specific angiogenesis inhibitor-1 expression in astrocytes and neurons: implications for its dual function as an apoptotic engulfment receptor. Brain Behav. Immun. 25, 915–921. https://doi.org/10.1016/j.bbi.2010.09.021.

Stephenson, J.R., Purcell, R.H., Hall, R.A., 2014. The BAI subfamily of adhesion GPCRs: synaptic regulation and beyond. Trends Pharmacol. Sci. 35, 208–215. https://doi.org/10.1016/j.tips.2014.02.002.

Toma, C., Hervas, A., Balmana, N., Vilella, E., Aguilera, F., Cusco, I., del Campo, M., Caballero, R., De Diego-Otero, Y., Ribases, M., Cormand, B., Bayes, M., 2011. Association study of six candidate genes asymmetrically expressed in the two cerebral hemispheres suggests the involvement of BAIAP2 in autism. J. Psychiatr. Res. 45, 280–282. https://doi.org/10.1016/j.jpsychires.2010.09.001.

Tsai, N.P., Wilkerson, J.R., Guo, W., Maksimova, M.A., DeMartino, G.N., Cowan, C.W., Huber, K.M., 2012. Multiple autism-linked genes mediate synapse elimination via proteasomal degradation of a synaptic scaffold PSD-95. Cell. 151, 1581–1594. https://doi.org/10.1016/j.cell.2012.11.040.

Tu, Y.K., Duman, J.G., Tolias, K.F., 2018. The adhesion-GPCR BAI1 promotes excitatory synaptogenesis by coordinating bidirectional trans-synaptic signaling. J. Neurosci. 38, 8388–8406. https://doi.org/10.1523/JNEUROSCI.3461-17.2018.

Varghese, M., Keshav, N., Jacot-Descombes, S., Warda, T., Wicinski, B., Dickstein, D.L., Harony-Nicolas, H., De Rubeis, S., Drapeau, E., Buxbaum, J.D., Hof, P.R., 2017. Autism spectrum disorder: neuropathology and animal models. Acta Neuropathol. 134, 537–566. https://doi.org/10.1007/s00401-017-1736-4.

Wojcik, S.M., Tantra, M., Stepniak, B., Man, K.N., Muller-Ribbe, K., Begemann, M., Ju, A., Papiol, S., Ronnenberg, A., Gurvich, A., Shin, Y., Augustin, I., Brose, N., Ehrenreich, H., 2013. Genetic markers of a Munc13 protein family member, BAIAP3, are gender specifically associated with anxiety and benzodiazepine abuse in mice and humans. Mol. Med. 19, 135–148. https://doi.org/10.2119/molmed.2013.00033.

Wong, J.C., Dutton, S.B., Collins, S.D., Schachter, S., Escayg, A., 2016. Huperzine A provides robust and sustained protection against induced seizures in Scn1a mutant mice. Front. Pharmacol. 7, 357. https://doi.org/10.3389/fphar.2016.00357.

Wong, J.C., Makinson, C.D., Lamar, T., Cheng, Q., Wingard, J.C., Terwilliger, E.F., Escayg, A., 2018. Selective targeting of Scn8a prevents seizure development in a mouse model of mesial temporal lobe epilepsy. Sci. Rep. 8, 126. https://doi.org/10.1038/s41598-017-17786-0.

Wong, J.C., Grieco, S.F., Dutt, K., Chen, L., Thelin, J.T., Inglis, G.A.S., Parvin, S., Garraway, S.M., Xu, X., Goldin, A.L., Escayg, A., 2021a. Autistic-like behavior, spontaneous seizures, and increased neuronal excitability in a Scn8a mouse model. Neuropsychopharmacology. https://doi.org/10.1038/s41386-021-00985-9.

Wong, J.C., Shapiro, L., Thelin, J.T., Heaton, E.C., Zaman, R.U., D'Souza, M.J., Murnane, K.S., Escayg, A., 2021b. Nanoparticle encapsulated oxytocin increases resistance to induced seizures and restores social behavior in Scn1a-derived epilepsy. Neurobiol. Dis. 147, 105147 https://doi.org/10.1016/j.nbd.2020.105147.

Yamaguchi, Y., Miura, M., 2015. Programmed cell death in neurodevelopment. Dev. Cell 32, 478–490. https://doi.org/10.1016/j.devcel.2015.01.019.

Yang, M., Crawley, J.N., 2009. Simple behavioral assessment of mouse olfaction. Curr. Protoc. Neurosci. https://doi.org/10.1002/0471142301.ns0824s48. Chapter 8, unit 8 24.

Yang, E.J., Ahn, S., Lee, K., Mahmood, U., Kim, H.S., 2016. Early behavioral abnormalities and perinatal alterations of PTEN/AKT pathway in Valproic acid Autism model mice. PLoS One 11, e0153298. https://doi.org/10.1371/journal.pone.0153298.

Zhang, Y., Chen, K., Sloan, S.A., Bennett, M.L., Scholze, A.R., O'Keeffe, S., Phatnani, H.P., Guarnieri, P., Caneda, C., Ruderisch, N., Deng, S., Liddelow, S.A., Zhang, C., Daneman, R., Maniatis, T., Barres, B.A., Wu, J.Q., 2014. An RNA-sequencing transcriptome and splicing database of glia, neurons, and vascular cells of the cerebral cortex. J. Neurosci. 34, 11929–11947. https://doi.org/10.1523/JNEUROSCI.1860-14.2014.

Zhang, X., Jiang, S., Mitok, K.A., Li, L., Attie, A.D., Martin, T.F.J., 2017. BAIAP3, a C2 domain-containing Munc13 protein, controls the fate of dense-core vesicles in neuroendocrine cells. J. Cell Biol. 216, 2151–2166. https://doi.org/10.1083/jcb.201702099.

Zhu, X.B., Wang, Y.B., Chen, O., Zhang, D.Q., Zhang, Z.H., Cao, A.H., Huang, S.Y., Sun, R. P., 2012. Characterization of the expression of macrophage inflammatory protein-1alpha (MIP-1alpha) and C-C chemokine receptor 5 (CCR5) after kainic acid-induced status epilepticus (SE) in juvenile rats. Neuropathol. Appl. Neurobiol. 38, 602–616. https://doi.org/10.1111/j.1365-2990.2012.01251.x.

Zhu, D., Li, C., Swanson, A.M., Villalba, R.M., Guo, J., Zhang, Z., Matheny, S., Murakami, T., Stephenson, J.R., Daniel, S., Fukata, M., Hall, R.A., Olson, J.J., Neigh, G.N., Smith, Y., Rainnie, D.G., Van Meir, E.G., 2015. BAI1 regulates spatial learning and synaptic plasticity in the hippocampus. J. Clin. Invest. 125, 1497–1508. https://doi.org/10.1172/JCI74603.

Zhu, D., Osuka, S., Zhang, Z., Reichert, Z.R., Yang, L., Kanemura, Y., Jiang, Y., You, S., Zhang, H., Devi, N.S., Bhattacharya, D., Takano, S., Gillespie, G.Y., Macdonald, T., Tan, C., Nishikawa, R., Nelson, W.G., Olson, J.J., Van Meir, E.G., 2018. BAI1 suppresses Medulloblastoma formation by protecting p53 from Mdm2-mediated degradation. Cancer Cell 33 (1004–1016), e5. https://doi.org/10.1016/j.ccell.2018.05.006.

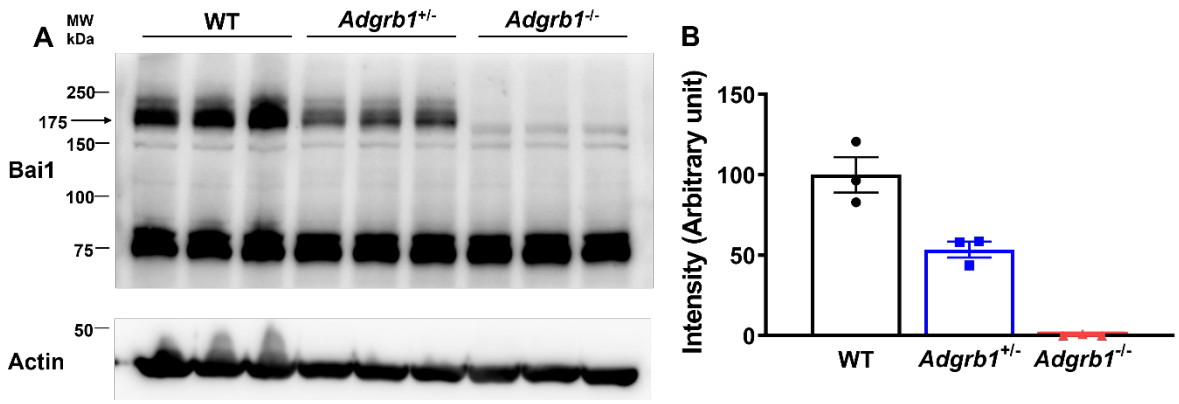

Supplementary Fig. 1. Brain expression of Bai1 in 5 month old *Adgrb1*$^{-/-}$, *Adgrb1*$^{+/-}$, and WT littermates. (A) Western blot performed with a C-terminal anti-Bai1 antibody showed that *Adgrb1*$^{-/-}$ mice lack expression of full-length Bai1 (~175 kDa). Of note, a smaller ~75 kDA band was also observed and may represent a non-specific band or a shorter Bai1 isoform. This band is equally abundant in all three genotypes indicating that it is not a cleaved form of the full-length Bai1. **(B)** *Adgrb1*$^{+/-}$ mutants express approximately 50% full length Bai1 levels when compared to WT littermates. WT, n = 3; *Adgrb1*$^{+/-}$, n = 3; *Adgrb1*$^{-/-}$, n = 3. Mean ± SEM.

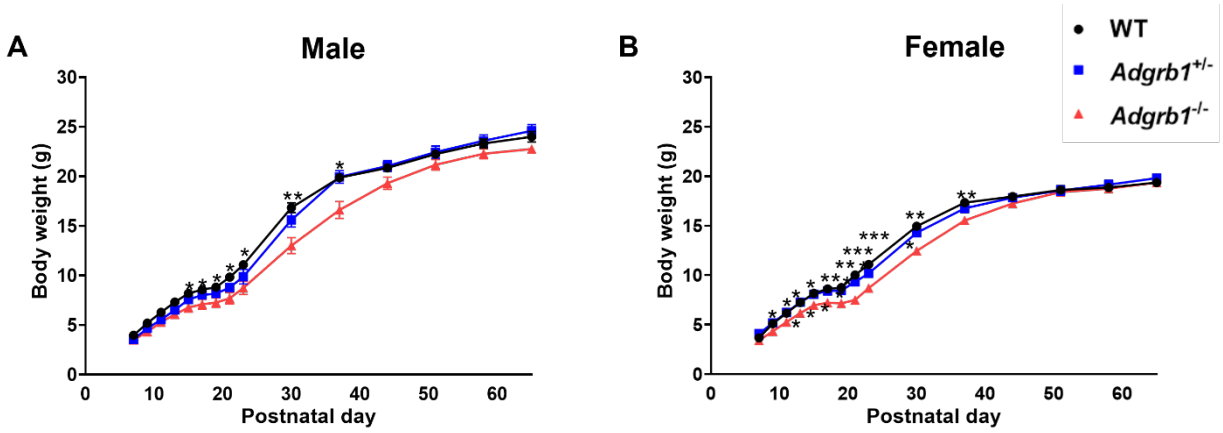

Supplementary Fig. 2. *Adgrb1*$^{-/-}$ mice show delayed growth. (A) *Adgrb1*$^{-/-}$ male and **(B)** female mice exhibit delayed growth compared to WT littermates until approximately P37. The growth rates of WT littermates and *Adgrb1*$^{+/-}$ were not significantly different. Male: WT, n = 15; *Adgrb1*$^{+/-}$, n = 11; *Adgrb1*$^{-/-}$, n = 10; Female: WT; n = 10; *Adgrb1*$^{+/-}$, n = 11; *Adgrb1*$^{-/-}$, n = 9. Mean ± SEM. *$p < 0.05$, **$p < 0.01$, ***$p < 0.001$, ****$p < 0.0001$. Statistical significance is based on comparisons within sex and across genotypes.

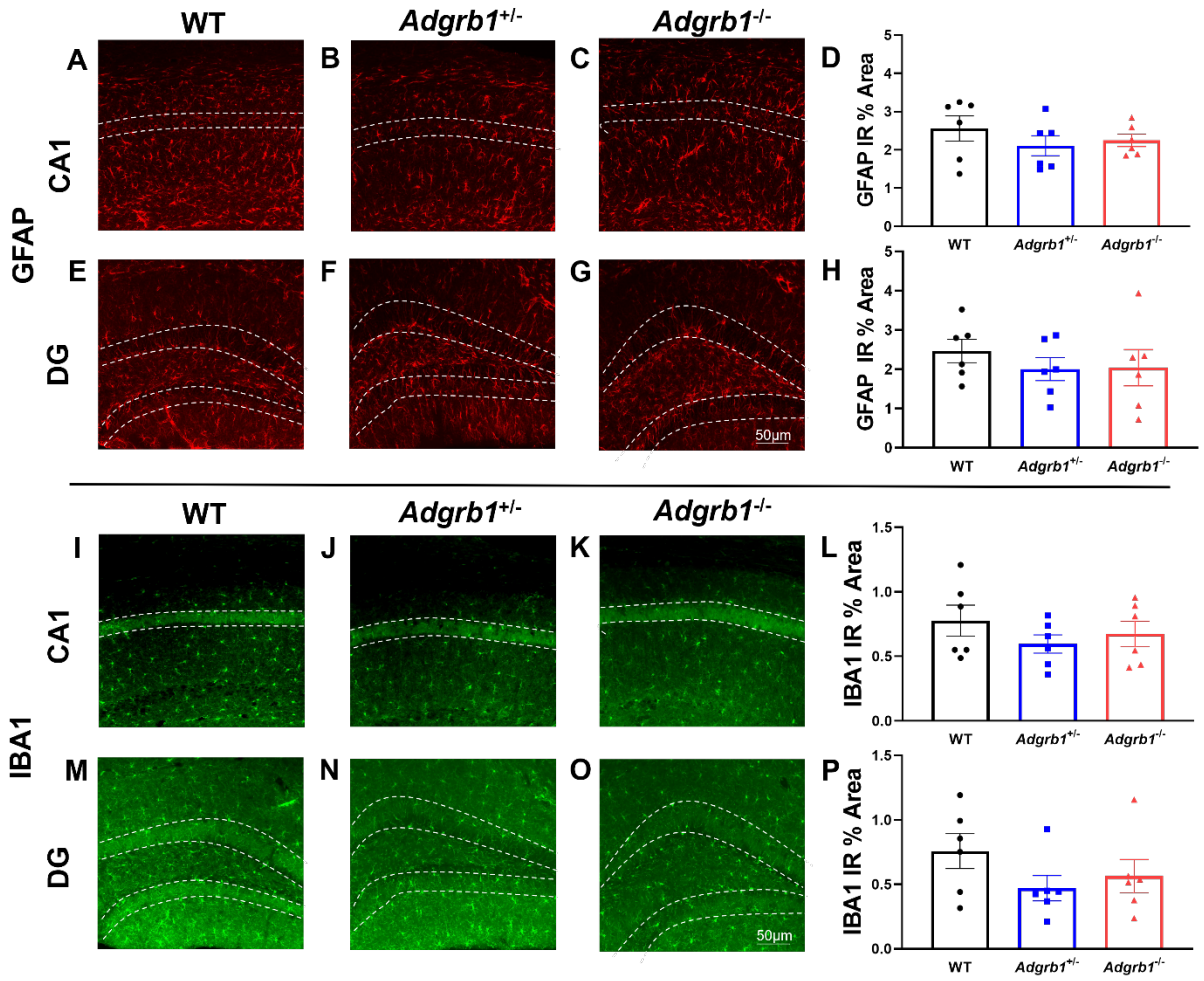

Supplementary Fig. 3. Levels of astrogliosis and microgliosis are comparable in 2-3 month old mice across all genotypes. No significant differences were observed between *Adgrb1*$^{+/-}$ and *Adgrb1*$^{-/-}$ mutants and WT littermates in **(A-H)** GFAP and **(I-P)** IBA1 immunoreactivity (IR). Dashed lines indicate the boundaries of the CA1 and DG regions. WT, n = 6; *Adgrb1*$^{+/-}$, n = 6; *Adgrb1*$^{-/-}$, n = 6. Mean ± SEM.

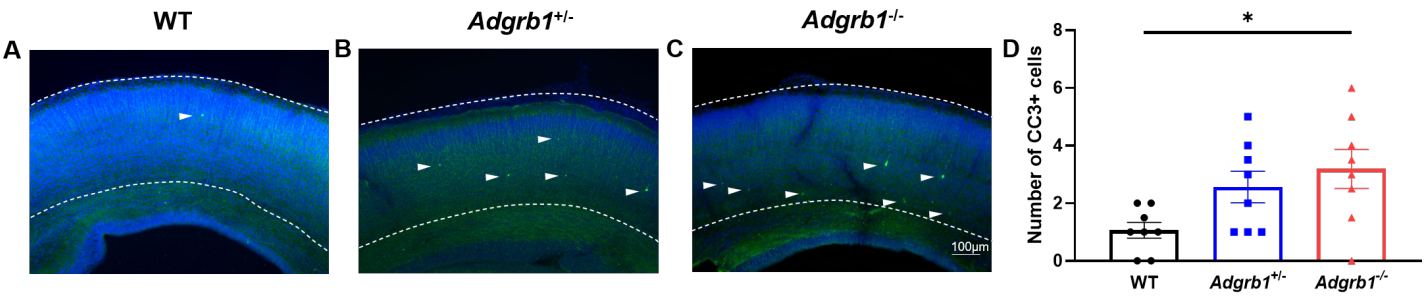

Supplementary Fig. 4. P1 *Adgrb1*$^{-/-}$ mice have more CC3+ cells in the primary somatosensory cortex compared to WT littermates. (A-C) Representative images of CC3+ cells in the primary somatosensory cortex. **(D)** *Adgrb1*$^{-/-}$ mice have more CC3+ cells than WT littermates. CC3+ cells are indicated by arrows. Dashed lines indicate the boundary of cortical layers I to VI. WT, n = 8; *Adgrb1*$^{+/-}$, n = 8; *Adgrb1*$^{-/-}$, n = 8. Mean ± SEM. *$p < 0.05$.

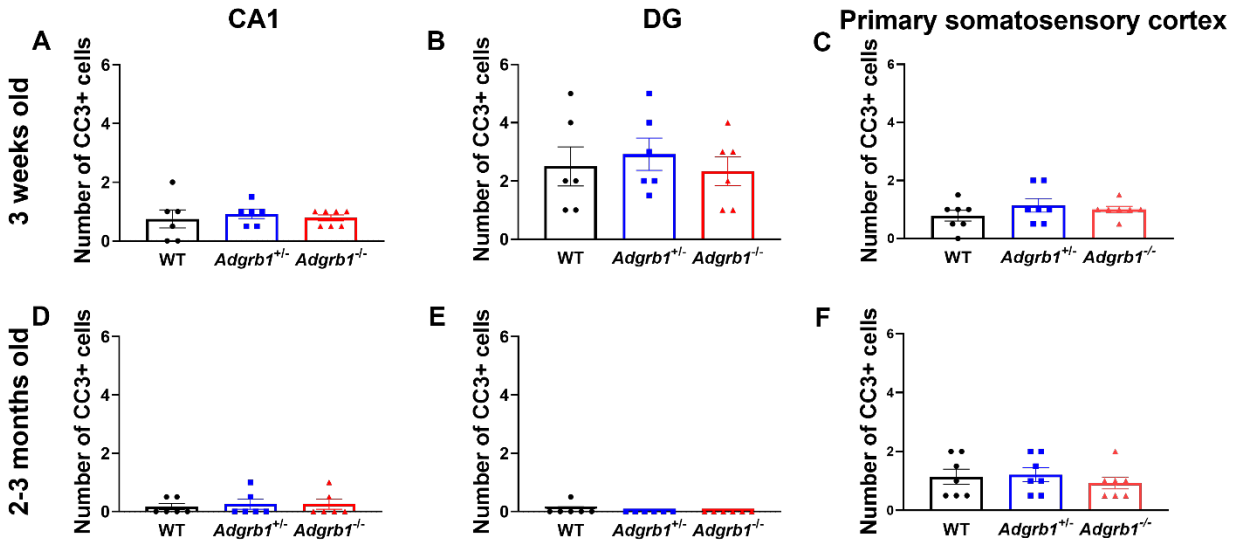

Supplementary Fig. 5. Number of CC3+ cells were comparable across genotypes in 3 week and 2–3 month old mice. No significant differences in the number of CC3+ cells were observed between genotypes in **(A-C)** 3 week and **(D-F)** 2-3 month old *Adgrb1*$^{+/-}$ and *Adgrb1*$^{-/-}$ mutants and WT littermates. WT, n = 6-7; *Adgrb1*$^{+/-}$, n = 6-7; *Adgrb1*$^{-/-}$, n = 6-7. Mean ± SEM.

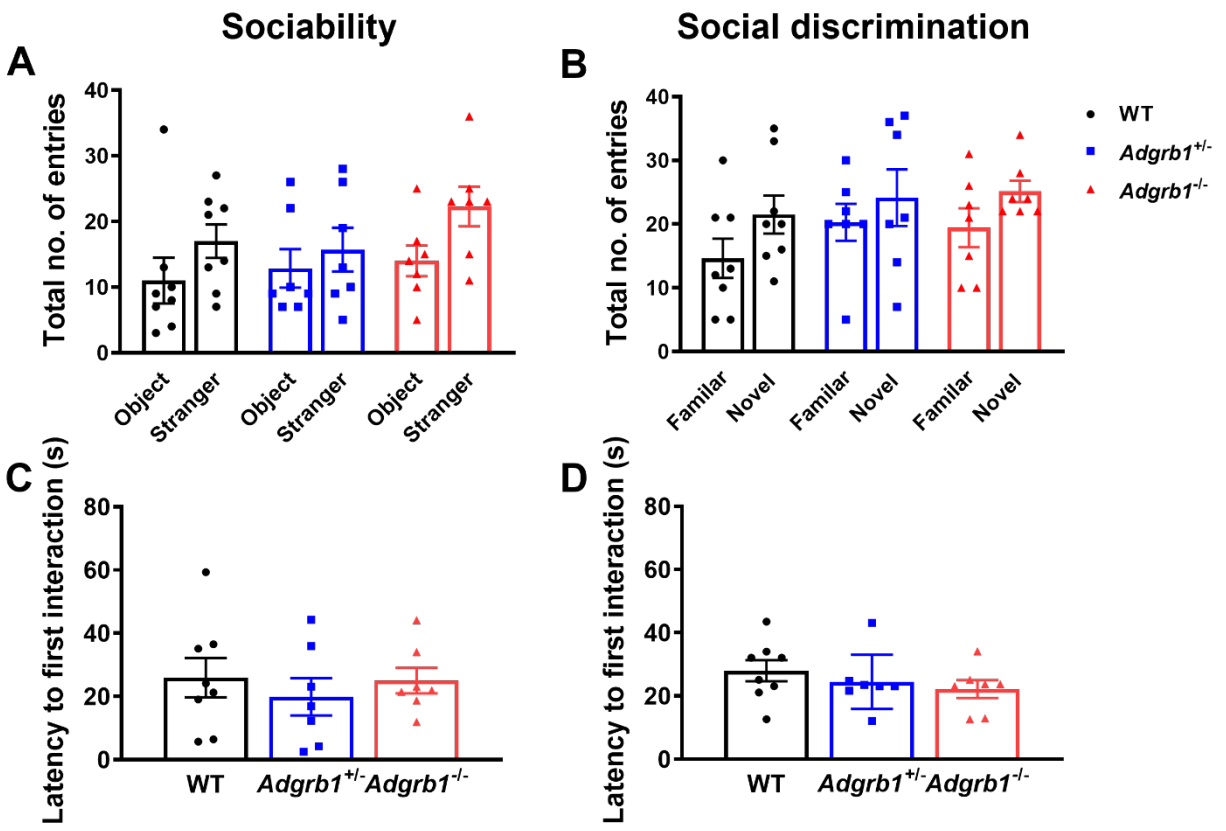

Supplementary Fig. 6. Total entries into each side chamber and average latency to the first interaction with either the stranger mouse or novel mouse was comparable between genotypes. (A-B) No significant differences were observed between genotypes in **(A)** the total number of entries into the side chambers containing the object or the stranger mouse during the sociability task, and **(B)** the side chambers with the familiar or novel mouse during the social discrimination task. **(C-D)** Latencies to the first interaction with the **(C)** stranger mouse or **(D)** novel mouse were similar for all genotypes in the sociability and social discrimination tasks, respectively. WT, n = 8; *Adgrb1*$^{+/-}$, n = 7; *Adgrb1*$^{-/-}$, n = 7. Mean ± SEM.

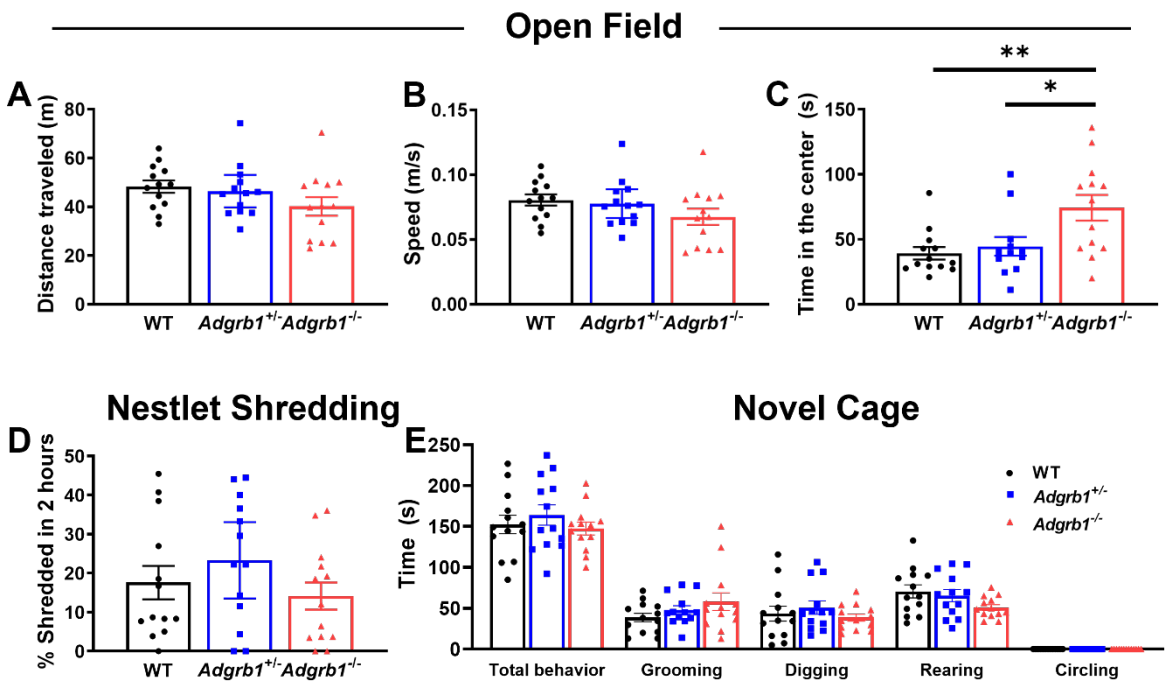

Supplementary Fig. 7. Male *Adgrb1*$^{-/-}$ mice and WT littermates show comparable behavior during open field exploration, nestlet shredding, and novel cage. (A-C) In the open field task, there was no significant effect of genotype on **(A)** total distance traveled, and **(B)** average speed. **(C)** *Adgrb1*$^{-/-}$ mutants spent significantly more time in the center of the open field. **(D)** In the nestlet shredding paradigm, there was no significant effect of genotype on the percentage of shredded nestlet during the 2-hour observation period. **(E)** In the novel cage paradigm, no significant differences were observed between *Adgrb1*$^{+/-}$ and *Adgrb1*$^{-/-}$ mutants and WT littermates in the time spent grooming, digging, rearing, and circling. WT, n = 13; *Adgrb1*$^{+/-}$, n = 13; *Adgrb1*$^{-/-}$, n = 13. Mean ± SEM.